Communication

High Entropy Alloys: Criteria for Stable Structure

SNEHASHISH TRIPATHY, GAURAV GUPTA, and SANDIP GHOSH CHOWDHURY

An effort has been made to reassess the phase predicting capability of various thermodynamic and topological parameters across a wide range of HEA systems. These parameters are valence electron concentration, atomic mismatch (δ), electronegativity difference ($\Delta\chi$), mixing entropy (ΔS_{mix}), entropy of fusion (ΔS_f), and mismatch entropy (S_σ). In continuation of that, two new parameters (a) Modified Darken–Gurry parameter ($\mathbf{A} = \boldsymbol{S\sigma^*\chi}$) and (b) Modified Mismatch Entropy parameter ($\mathbf{B} = \boldsymbol{\delta^* S\sigma}$) have been designed to predict the stable crystal structure that would form in the HEA systems considered for assessment.

https://doi.org/10.1007/s11661-017-4388-z

'High Entropy Alloys' (HEA) represent a recent class of materials which constitute multiple principal elements in equiatomic or non-equiatomic proportions. The presence of a number of principal elements, particularly in equiatomic proportion, leads to a large configurational entropy and thus, high entropy of mixing. Consequently, these alloys tend to form solid solutions with simple crystal structures like FCC, BCC, or a mixture of both, rather than intermetallics or other complex phases.[1–4] A variety of HEAs have been explored till date and it has been reported that these alloys exhibit very promising properties like high strength, ductility, excellent fracture toughness at cryogenic temperatures (*i.e.*, ≤ 77 K),[5] good resistance to wear, oxidation, and high temperature softening. These properties are directly related to the underlying crystal structure of the solid-solution phase. However, due to the absence of reliable information about the phase diagrams of multicomponent systems, the knowledge about phase formation in such systems is restrictively dependent upon the experimental determination. Lately, in order to tackle this present limitation of classical thermodynamics-based phase prediction, there have been various attempts by researchers to lay down certain thumb rules for phase formation based upon first principle calculations, **Cal**culation of **Ph**ase **D**iagram (CALPHAD) principles, as well as other thermodynamic and topological parametric approaches.[6–17]

The existing phase prediction techniques range from the first principle-based DFT calculations to CALPHAD-based Phase Diagram Evaluation techniques.[18–22] The first principle-based calculations are very much computationally intensive; however, these are the most efficient techniques when it comes to determination of ground-state crystal structure. These basically involve the solution of the Kohn–Sham formulation[23] which is a minimization procedure of a coupled set of Schrodinger Equations for each electron in the system; being solved individually, yet self-consistently for the electron density, $\rho(r)$. The Kohn–Sham formulation is expressed as mentioned in Eq. [1], where the first term on the left represents kinetic energy of a single electron; the second term defines electron–ion coupling potential; the third term reflects the electron–electron interaction; and the fourth term is for the exchange correlation potential[18]:

$$\left\{\left[\frac{-h^2}{2m}\left(\nabla^2 r\right)\right] + V_e(r) + \int \mathrm{d}r \frac{\rho(r')}{|r-r'|} + V_{xc}[\rho(r)]\right\}\Psi_i(r) = \epsilon_i \Psi i(r) \quad [1]$$

The Kohn–Sham formulation assumes an initial crystal structure depending upon the symmetry of which the single-electron wave function is formulated in a plane wave basis. This is followed by the adoption of an approximation technique (like Local Density Approximation or Generalized Gradient Approximation) to obtain the exchange correlation potential and finally by selection of a technique to determine the electron–ion coupling potential. This formulation is then solved to obtain the lowest energy structure in the $T \approx 0$K limit. The obtained energy can be scaled to any finite temperature using Cluster Expansion models which take care of the various entropy contributions to the total energy with increasing temperature. The greatest advantage of using DFT for the ground-state structure prediction is the ability to evaluate the total energy across a spectrum of crystal structures, some of them being even hypothetical.[19,20]

Another method for prediction of stable phases in such alloys is the **Cal**culation of **Ph**ase **D**iagram technique (CALPHAD). CALPHAD makes use of the Gibbs energy minimization principle to determine the stable and metastable structures that would form in a system.[21,22,24] In this technique, the Gibbs energy of a

SNEHASHISH TRIPATHY and SANDIP GHOSH CHOWDHURYare with the Materials Engineering Division, CSIR-National Metallurgical Laboratory, Jamshedpur, 831007, India. Contact e-mail: sandipgc@gmail.com GAURAV GUPTA is with the School of Materials Science & Technology, IIT BHU, Varanasi.

Manuscript submitted June 5, 2017.
Article published online November 7, 2017

particular phase is expressed in the form a Redlich–Kister-type equation as given in Eq. [2], where the first term depicts the contribution of the pure components present in the phase, the second term signifies the ideal mixing contribution to Gibbs energy, and the third and fourth terms are the excess Gibbs energy of mixing calculated by using the binary and ternary interactions among the components.[24,25]

$$G_{phase} = \sum_i X_i G_i^0 + \sum_i X_i ln X_i + \sum_i \sum_{j>i} X_i X_j \sum_n \omega_{ij}^n (X_i - X_j)^n + \sum_i \sum_{j>i} \sum_{k>j} L_{ijk} X_i X_j X_k. \quad [2]$$

A recent work by Raghavan *et al.*[7] in predicting the stable crystal structure using the CALPHAD approach has revealed more accurate prediction for the BCC phase than the FCC. This has been attributed to the inability of CALPHAD to deal with kinetic effects which have a more dominant role to play in the formation of latter crystal structure. Currently, there exist dedicated databases of various thermodynamic parameters for multicomponent-based HEAs which take into account all possible binary interactions and tentatively the involved ternary ones as well.[26] However, there is a lack of good-quality data on ternary interactions especially at low temperatures and therefore, the structure prediction is still dependent on various extrapolation schemes. This is the reason why in certain cases CALPHAD predictions do not match with the experimentally obtained structure of various phases. Some of the examples of such ambiguity include the CoReRuV system which forms a complex multiphase structure in contrast to the single-phase HCP structure predicted by CALPHAD.[27] Similarly, in CoCrCuFeMn and CoCrMnNiV systems, CALPHAD predictions underestimate the low-temperature thermal stability of the sigma (σ) phase, which has been observed experimentally.[28] Although the above-mentioned examples utilize the TCNI database of different versions, it has to be understood that the present HEA databases are not very different and derive much of its data from the TCNI and other similar databases, hence inherit the limitations as well. The problem would pertain until the databases contain either experimental or first principle-based data for binary and ternary interactions across the entire composition range of a given system. Thus, a combination of DFT-based approach and CALPHAD can prove to be an extremely powerful technique in predicting the stable structures in multicomponent systems. However, until this combined approach becomes an exhaustive technique, the use of various thermodynamic and topological parameters for prediction of stable crystal structure would gain popularity. These parameters are essentially one or the other form of the various metallurgical parameters that were laid down by Hume Rothery as 'Rules for Solid Solution Formation' which in a very broad sense may be stated as follows[29–31]:

- Atomic size difference of the components—solid solubility of the solute ceases as soon as the atomic size of the solute differs from that of the solvent by more than 15 pct.
- Electrochemical difference among the components—larger the difference in chemical affinity of solute and solvent, higher is the tendency towards formation of intermediate compounds rather than solid solutions.
- Electron concentration change on alloying—the extent of solid solution in a solvent of lower valence is always greater than the *vice versa*.

All such parameters being a formulation of either one or a combination of few of the Hume Rothery rules, are applicable only for room-temperature stable phase prediction. The important thing that has to be understood with respect to various such parameters is that they represent mere thumb rules based upon certain functions which intuitively can be related to either first principle-based outcomes like kinetic energy of electrons (reflected by VEC) or CALPHAD-based outcomes like Gibbs energy of the system (reflected by Mismatch Entropy). One strong limitation of such parameters is their incapability to predict the formation of complex crystal structures in multicomponent alloys like the sigma and the Laves phases, etc. These parameters will only act as a thumb rule in case of predicting simple ground-state structures like FCC and BCC at room temperature.

In the present work, an effort has been made to reassess the phase predicting capability of various such thermodynamic and topological parameters across a wide range of HEA systems. In continuation of the present effort, two new parameters have also been designed to predict the stable crystal structure that would form in the HEA systems considered for assessment.

The already existing parameters which have been reassessed are valence electron concentration (VEC), atomic mismatch (δ), electronegativity difference ($\Delta\chi$), mixing entropy (ΔS_{mix}), entropy of fusion (ΔS_f), and mismatch entropy (S_σ). The two new parameters formulated are the Modified Darken–Gurry parameter (**A**) and the Modified Mismatch Entropy parameter (**B**). Most of these parameters have been used in the previous studies for predicting whether the system will form a solid solution or an intermetallic or an amorphous phase with only a few attempts for crystal structure prediction.[10,11,29,32–37] In the present work, these parameters are computed for over 150 different HEA systems whose stable crystal structures have already been reported in literature elsewhere.[7,38–41] These parameters are then plotted individually in a 1D map. Based upon certain thresholding, the regimes for different crystal structures (FCC, BCC, and FCC + BCC) are demarcated with an attempt to explain the underlying principle.

The HEA systems under consideration consist of a combination of elements (listed in Table I) in different proportions. Among the systems chosen for study, 53 have FCC, 42 have FCC + BCC, and 58 have BCC as

Table I. List of Elements Present in the HEA Systems Considered Along with Some of Their Properties

Element	Atomic No.	VEC	Atomic Radii(Å)	Elec. Neg	S_{fusion}/R
Al	13	3	1.432	1.61	1.38
Co	27	9	1.251	1.88	1.0925
Cr	24	6	1.249	1.66	1.1586
Cu	29	11	1.278	1.9	1.17464
Fe	26	8	1.241	1.83	0.9172
Mn	25	7	1.35	1.55	1.0222
Mo	42	6	1.363	2.16	1.5566
Ni	28	10	1.246	1.91	1.2167
Ti	22	4	1.462	1.54	0.87684
W	74	6	1.367	2.36	1.702
Zn	30	12	1.395	1.65	1.271
V	23	5	1.316	1.63	1.2562
Nb	41	5	1.429	1.6	1.312
Ta	73	5	1.43	1.5	1.337
Hf	72	4	1.578	1.3	1.3055
Zr	40	4	1.603	1.33	0.791

the stable crystal structure (experimentally proven). Some of the input values used for the computation of various parameters *viz*. atomic radii, electronegativity, VEC, ΔS_f are also listed in Table I.

1: Valence Electron Concentration (VEC): This parameter is basically the integration of the density of states (DOS) of s-, p-, and d-electrons in the valence band of a particular element.[9,10,42] The VEC value in case of iron, for example is 8 as its configuration in the outer shells is $4s^2\ 3d^6$. So, by adding up the 4s and 3d electrons, it gives the VEC value of 8. Thus for the overall system, this is calculated using the VEC values of individual elements as presented in Eq. [3].

$$VEC = \sum_{i=1}^{N} C_i * VEC_i \qquad [3]$$

C_i in all cases represents the atomic fraction of the *i*th component.

2: Atomic mismatch (δ): This is basically the measure of difference in atomic size values of constituent elements from the mean size as presented in Eq. [4].

$$\delta = 100 * \sqrt{\sum_{i=1}^{N} C_i * \left(1 - \left(\frac{r_i}{\bar{r}}\right)^2\right)}, \qquad [4]$$

where r_i is the atomic radii of constituent element and $\bar{r} = \sum_{i=1}^{N} C_i * r_i$.

3: Electronegativity difference ($\Delta\chi$): This is basically the measure of difference in electronegativity of each constituent component from the mean electronegativity of the system as presented in Eq. [5].

$$\chi = \sum_{i=1}^{N} C_i * (\chi_i - \bar{\chi})^2 \qquad [5]$$

where $\bar{\chi} = \sum_{i=1}^{N} C_i\chi_i$ and χ_i is the Pauling Electronegativity of the *i*th component.

4: Mismatch Entropy (S_σ): This parameter signifies the change in entropy due to atomic size mismatch. High value of mismatch entropy means the change in overall entropy due to difference in atomic sizes is more. Hence, it can be inferred that there will be less number of total possible indistinguishable arrangements and thus, lesser overall configurational entropy. This parameter has been formulated as given in Eq. [6] by Mansoori *et al.*,[43] based on the model of mixture consisting of hard spheres.

$$S_\sigma = k * \left[\frac{3}{2}(\zeta^2 - 1)y_1 + \frac{3}{2}(\zeta - 1)^2 y_2 - \frac{1}{2}\{(\zeta - 1)(\zeta - 3) + \ln\zeta\}(1 - y_3)\right] \qquad [6]$$

where $\zeta = \frac{1}{1-\xi}$ and $\xi = 0.64$ for dense pack solids. The terms, y_1 and y_2 are actually directly proportional to the square of the difference in the atomic sizes and y_3 is simply a ratio of the projected area and volume of different atoms each raised to an exponent of 3 and 2, respectively. For the calculation of y_1, y_2, and y_3, the value of atomic diameter (d_i) of each constituent component have been used.

5: Entropy of mixing (ΔS_{mix}): The configurational entropy attained by the system is defined as given below in Eq. [7],

$$\Delta S_{mix} = -R * \sum_{i=1}^{N} C_i * \ln C_i, \qquad [7]$$

where R is the universal gas constant and C_i is the concentration on each element present in the system.

6: Entropy of Fusion (ΔS_f): This depicts the change in the entropy of the system when there is a phase transformation from liquid to solid or *vice versa*. For the overall alloy system, it is computed as given in Eq. [8],

$$\Delta S_f = \sum_{i=1}^{N} C_i * S_f^i, \qquad [8]$$

where S_f^i is the entropy of fusion of individual element.

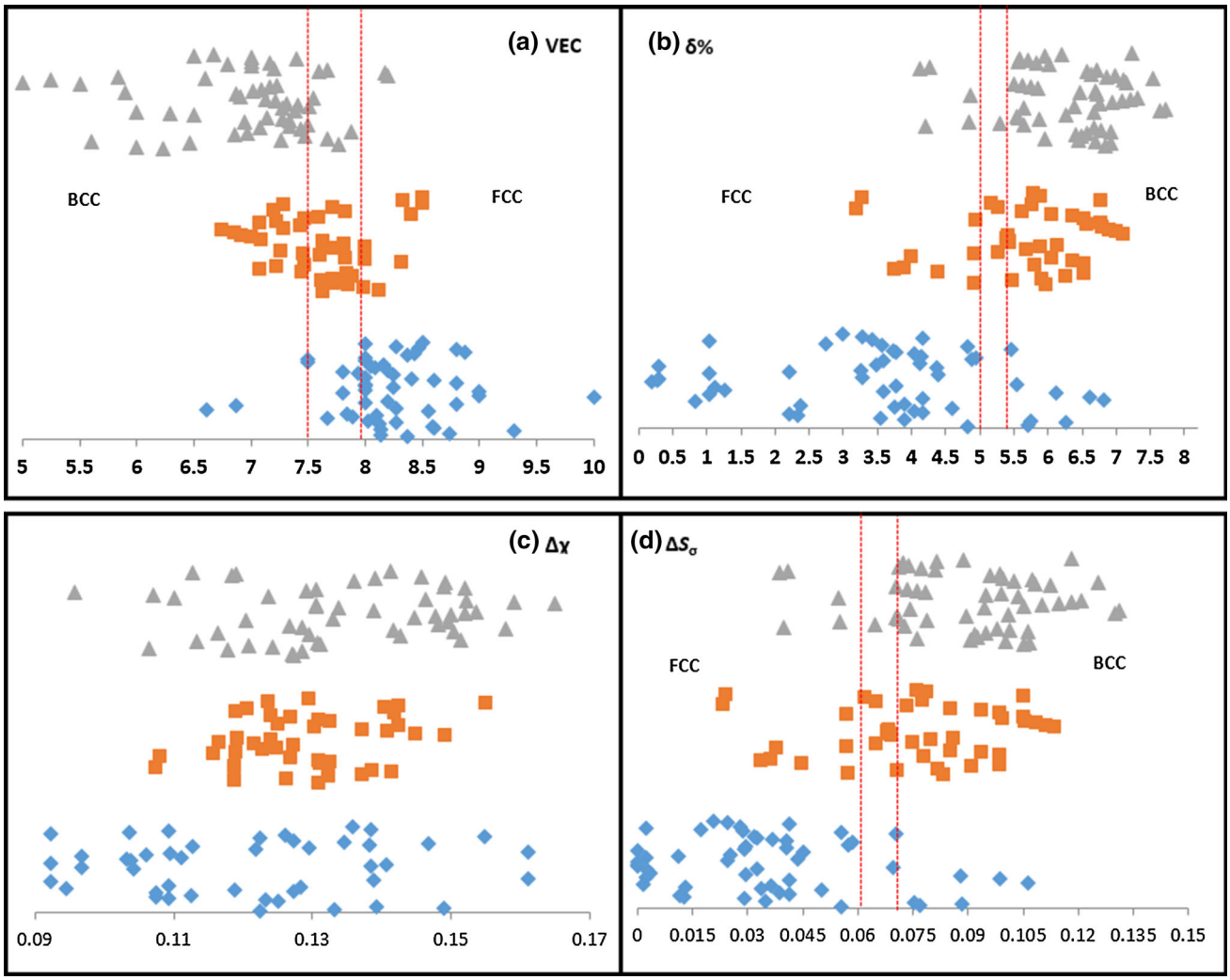

Fig. 1—1D maps of the computed values of (*a*) VEC, (*b*) δ pct, (*c*) $\Delta\chi$, and (*d*) ΔS_σ. (Triangles represent BCC phase, rhombi represent FCC phase, and squares represent mixed FCC + BCC phase).

Each parameter calculated using the equations given above is tabulated in Table II and 1D maps for each parameter was plotted where a particular type of crystal structure was assigned a unique representation. The analysis of the spread and the trend of each of the parameters were done to threshold it into different crystal structure regimes. Figures 1 represents the 1D maps of the computed values of VEC, δ, $\Delta\chi$, and S_σ. The plots for VEC, Atomic mismatch, and Mismatch entropy show a good representation of demarcation of the various phase regimes in the systems considered. As reported earlier,[9–11] the systems with lower VEC tend to form BCC and those with higher values tend to form FCC. Here, it can be seen that VEC values less than 7.5 favor the BCC structure and values higher than 7.9 favor the FCC. This may be attributed to the fact that the Brillouin zones of the noble metals are only partially filled with electrons; although they are touched by the Fermi surface, they are not overlapped as it happens in the case of the transition elements (or elements with higher valence). Thus, when the value of VEC is low, the presence of low valence components is higher which yields a low e/a ratio or in other words lesser number of loosely bound electrons. Therefore, the peak of DOS for the electrons in the space where the Brillouin zone and Fermi surface interact (which is basically a representation of kinetic energy of electrons), occurs at lower energy levels. Since the electrons to be accommodated already possess a lower total energy, the crystal structure can be of a more open nature, *i.e.*, the BCC. In case of higher VEC due to the higher number of loosely bound electrons or greater extent of overlapping of the Brillouin zone and Fermi surface (due to higher fraction of high valence components), the peak of DOS for the electrons occurs at higher energy levels and thus, the electrons which have to be accommodated are present with a higher total energy. This ultimately means that the crystal structure has to be of a closed nature (*i.e.*, FCC) so as to minimize the kinetic energy of the electrons.[10,11,30,31,42]

The atomic mismatch, δ values indicate that higher values favor the BCC phase, whereas the FCC phase is

Table II. Comparison of Base Structure of Various Systems Using VEC, Atomic Mismatch, Mismatch Entropy, Modified Darken–Gurry Parameter, and Modified Mismatch Entropy Parameter

Sl No	Systems	Exp Phase	VEC	Predicted	Atomic Mis	Predicted	Entpmis	Predicted	Eng*Smis	Predicted	Atm*Smis	Predicted	Synthesis Route
1	CoCrCuFeNiTi0.5	FCC	8.36	FCC	4.822	FCC + BCC	0.056	FCC	0.007	FCC + BCC	0.268	FCC + BCC	Casting
2	CoCrCuFeNiTi0.8	FCC	8.14	FCC	5.700	BCC	0.077	FCC	0.010	BCC	0.438	BCC	Casting
3	Cu2.5NiCoZnAlTi	FCC	8.73	FCC	6.263	BCC	0.088	FCC	0.013	BCC	0.553	BCC	MA
4	Cu5NiCoZnAlTi	FCC	9.30	FCC	5.747	BCC	0.075	FCC	0.011	BCC	0.434	BCC	MA
5	Ni2.5FeCrCoMnW	FCC	8.13	FCC	3.900	FCC	0.035	FCC	0.008	FCC + BCC	0.135	FCC	MA
6	Ni5FeCrCoMnW	FCC	8.60	FCC	3.553	FCC	0.029	FCC	0.006	FCC + BCC	0.103	FCC	MA
7	NiCrCuFeMo0.25	FCC	8.59	FCC	2.327	FCC	0.013	FCC	0.002	FCC	0.029	FCC	MA
8	NiCoCrFeMo0.25	FCC	8.12	FCC	2.201	FCC	0.011	FCC	0.001	FCC	0.025	FCC	MA
9	Al0.5CoCrCuFeNi	FCC	8.27	FCC	4.169	FCC	0.041	FCC	0.005	FCC	0.172	FCC	Casting
10	Al0.375CoCrFeNi	FCC	8.03	FCC	4.046	FCC	0.039	FCC	0.004	FCC	0.157	FCC	Casting
11	Al0.5CrFeCoNi	FCC	7.67	FCC + BCC	4.602	FCC + BCC	0.050	FCC	0.006	FCC + BCC	0.231	FCC + BCC	Casting
12	CoCrFeNiAl0.3	FCC	7.88	FCC + BCC	3.758	FCC	0.034	FCC	0.004	FCC	0.127	FCC	Casting
13	CoCrFeNiMo0.3	FCC	8.09	FCC	2.378	FCC	0.013	FCC	0.002	FCC	0.031	FCC	Casting
14	CoCrFeNiAl0.3Mo0.1	FCC	7.84	FCC + BCC	3.903	FCC	0.036	FCC	0.004	FCC	0.142	FCC	Casting
15	FeCoNiCrCu0.5	FCC	8.56	FCC	0.835	FCC	0.002	FCC	0.000	FCC	0.001	FCC	Casting
16	Ti0.5CrFeCoNiAl0.25Cu0.75	FCC	6.61	BCC	6.813	BCC	0.106	FCC + BCC	0.014	BCC	0.725	BCC	Casting
17	Al0.5CoCrCuFeNi	FCC	8.27	FCC	4.169	FCC	0.041	FCC	0.005	FCC	0.172	FCC	Casting
18	Cu0.5NiAlCoCrFeTiMo	FCC	6.87	BCC	6.611	BCC	0.099	FCC + BCC	0.019	BCC	0.653	BCC	MA
19	CoCrCuFeNi	FCC	8.80	FCC	1.033	FCC	0.002	FCC	0.000	FCC	0.002	FCC	Casting
20	CoCrCuFeNiTi	FCC	8.00	FCC	6.117	BCC	0.088	FCC	0.012	BCC	0.537	BCC	Casting
21	FeNiCrCuMo	FCC	8.20	FCC	3.580	FCC	0.029	FCC	0.005	FCC	0.105	FCC	Casting
22	CuNi	FCC	10.50	FCC	1.268	FCC	0.004	FCC	0.000	FCC	0.005	FCC	MA
23	CuNiCo	FCC	10.00	FCC	1.117	FCC	0.003	FCC	0.000	FCC	0.003	FCC	MA
24	CuNiCoZn	FCC	9.00	FCC	3.781	FCC	0.033	FCC	0.007	FCC + BCC	0.123	FCC	MA
25	CuNiCoZnAl	FCC	7.80	FCC + BCC	5.549	BCC	0.070	FCC	0.017	BCC	0.386	BCC	MA
26	NiFe	FCC	9.00	FCC	0.201	FCC	0.000	FCC	0.000	FCC	0.000	FCC	MA
27	NiFeCr	FCC	8.00	FCC	0.265	FCC	0.000	FCC	0.000	FCC	0.000	FCC	MA
28	NiFeCrCo	FCC	8.25	FCC	0.302	FCC	0.000	FCC	0.000	FCC	0.000	FCC	MA
29	NiFeCrCoMn	FCC	8.00	FCC	3.269	FCC	0.025	FCC	0.003	FCC	0.080	FCC	MA
30	FeNiMn	FCC	8.00	FCC	4.392	FCC	0.044	FCC	0.006	FCC + BCC	0.192	FCC	MA
31	NiCoCrCuFe	FCC	8.80	FCC	1.033	FCC	0.002	FCC	0.000	FCC	0.002	FCC	MA
32	CoFeNiCuV	FCC	8.60	FCC	2.203	FCC	0.011	FCC	0.001	FCC	0.024	FCC	Casting
33	CoCrFeNiCu0.75Al0.25	FCC	8.40	FCC	3.250	FCC	0.025	FCC	0.003	FCC	0.082	FCC	Casting
34	CoCrFeNiCu0.5Al0.5	FCC	8.00	FCC	4.370	FCC	0.045	FCC	0.005	FCC + BCC	0.198	FCC	Casting
35	CoCrFeNi	FCC	8.25	FCC	0.302	FCC	0.000	FCC	0.000	FCC	0.000	FCC	Casting
36	CoCrFeNiAl0.25	FCC	7.94	FCC + BCC	3.478	FCC	0.029	FCC	0.003	FCC	0.101	FCC	Casting
37	CoCrFeNiAl0.375	FCC	7.80	FCC + BCC	4.117	FCC	0.040	FCC	0.004	FCC	0.167	FCC	Casting
38	MoCrFeNiCu	FCC	8.20	FCC	3.580	FCC	0.029	FCC	0.005	FCC	0.105	FCC	Casting
39	Ti0.5Co1.5CrFeNi1.5	FCC	8.09	FCC	4.885	FCC + BCC	0.057	FCC	0.007	FCC + BCC	0.280	FCC + BCC	Casting
40	Ti0.5Co1.5CrFeNi1.5Mo0.1	FCC	8.05	FCC	4.938	FCC + BCC	0.058	FCC	0.008	FCC + BCC	0.288	FCC + BCC	Casting
41	CoCrFeNiCuAl0.5V0.2	FCC	8.16	FCC	4.146	FCC	0.041	FCC	0.005	FCC	0.168	FCC	Casting
42	Fe4Mn4Co1Cr1	FCC	7.50	FCC + BCC	4.045	FCC	0.037	FCC	0.005	FCC + BCC	0.149	FCC	Casting
43	Fe3Mn3Ni2Co1Cr1	FCC	8.00	FCC	3.778	FCC	0.032	FCC	0.005	FCC	0.123	FCC	Casting
44	Fe3Mn3Co2Cr2	FCC	7.50	FCC + BCC	3.738	FCC	0.032	FCC	0.004	FCC	0.119	FCC	Casting

Table II. Continued

Sl No	Systems	Exp Phase	VEC	Predicted	Atomic Mis	Predicted	Entpmis	Predicted	Eng*Smis	Predicted	Atm*Smis	Predicted	Synthesis Route
45	Ti0.5CoCrFeNiCu0.75Al0.25	FCC	8.00	FCC	5.459	FCC + BCC	0.070	FCC	0.009	FCC + BCC	0.384	BCC	Casting
46	Ti0.5CoCrFeNiCu	FCC	8.36	FCC	4.822	FCC + BCC	0.056	FCC	0.007	FCC + BCC	0.268	FCC + BCC	Casting
47	Mn2CrFeNi2Cu	FCC	8.43	FCC	3.568	FCC	0.029	FCC	0.004	FCC	0.103	FCC	Casting
48	MnCrFe2Ni2Cu2	FCC	8.88	FCC	2.748	FCC	0.017	FCC	0.002	FCC	0.048	FCC	Casting
49	CoCrFeNiCu	FCC	8.80	FCC	1.033	FCC	0.002	FCC	0.000	FCC	0.002	FCC	Casting
50	CoCrFeNiCuAl0.3	FCC	8.47	FCC	3.423	FCC	0.028	FCC	0.003	FCC	0.095	FCC	Casting
51	CoCrFeNiCuAl0.5	FCC	8.27	FCC	4.169	FCC	0.041	FCC	0.005	FCC	0.172	FCC	Casting
52	CoCrFeNiMn	FCC	8.00	FCC	3.269	FCC	0.025	FCC	0.003	FCC	0.080	FCC	Casting
53	CoCrFeNiMnCu	FCC	8.50	FCC	2.997	FCC	0.021	FCC	0.003	FCC	0.062	FCC	Casting
54	Ti0.5CrFeCoNiAl0.5Cu0.5	FCC + BCC	7.64	FCC + BCC	5.968	BCC	0.083	FCC	0.011	BCC	0.497	BCC	Casting
55	Al0.5CoCrCuFeNiTi0.2	FCC + BCC	8.12	FCC	4.931	FCC + BCC	0.057	FCC	0.007	FCC + BCC	0.283	FCC + BCC	Casting
56	Al0.5CoCrCuFeNiTi0.4	FCC + BCC	7.98	FCC + BCC	5.491	FCC + BCC	0.071	FCC	0.009	FCC + BCC	0.389	BCC	Casting
57	Al0.5CoCrCuFeNiTi0.6	FCC + BCC	7.85	FCC + BCC	5.922	BCC	0.082	FCC	0.011	BCC	0.485	BCC	Casting
58	Al0.5CoCrCuFeNiTi0.8	FCC + BCC	7.73	FCC + BCC	6.262	BCC	0.091	FCC + BCC	0.013	BCC	0.571	BCC	Casting
59	Al0.5CoCrCuFeNiTi	FCC + BCC	7.62	FCC + BCC	6.535	BCC	0.099	FCC + BCC	0.014	BCC	0.645	BCC	Casting
60	Al0.3CrFe1.5MnNi1.5	FCC + BCC	7.72	FCC + BCC	4.400	FCC + BCC	0.045	FCC	0.006	FCC + BCC	0.197	FCC	Casting
61	Al0.3CoCrFeNi	FCC + BCC	7.88	FCC + BCC	3.758	FCC	0.034	FCC	0.004	FCC	0.127	FCC	Casting
62	Al0.3CoCrFeNiMo0.1	FCC + BCC	7.84	FCC + BCC	3.903	FCC	0.036	FCC	0.004	FCC	0.142	FCC	Casting
63	Cu0.5CoNiCrAl	FCC + BCC	7.44	BCC	5.805	BCC	0.078	FCC	0.010	BCC	0.452	BCC	Casting
64	Ti0.5CrFeNiAlCo1.5	FCC + BCC	7.08	BCC	6.536	BCC	0.099	FCC + BCC	0.013	BCC	0.644	BCC	Casting
65	Ti0.5CrFeNiAlCo2	FCC + BCC	7.23	BCC	6.364	BCC	0.094	FCC + BCC	0.012	BCC	0.597	BCC	Casting
66	Ti0.5CrFeNiAlCo3	FCC + BCC	7.47	BCC	6.050	BCC	0.085	FCC	0.011	BCC	0.516	BCC	Casting
67	Al0.45FeNiCrCuCo	FCC + BCC	8.32	FCC	4.007	FCC	0.038	FCC	0.004	FCC	0.153	FCC	MA
68	CoCrFeNiCuAl0.8	FCC + BCC	8.00	FCC	4.922	FCC + BCC	0.057	FCC	0.007	FCC + BCC	0.280	FCC + BCC	Casting
69	CoCrFeNiCuAl	FCC + BCC	7.83	FCC + BCC	5.281	FCC + BCC	0.065	FCC	0.008	FCC + BCC	0.344	FCC + BCC	Casting
70	CoCrFeNiCuAl1.3	FCC + BCC	7.60	FCC + BCC	5.686	BCC	0.075	FCC	0.009	FCC + BCC	0.426	BCC	Casting
71	CoCrFeNiCuAl1.5	FCC + BCC	7.46	BCC	5.893	BCC	0.080	FCC	0.010	BCC	0.472	BCC	Casting
72	CoCrFeNiCuAl1.8	FCC + BCC	7.26	BCC	6.133	BCC	0.086	FCC	0.011	BCC	0.529	BCC	Casting
73	Co0.5CrFeNiCuAl	FCC + BCC	7.73	FCC + BCC	5.448	FCC + BCC	0.069	FCC	0.008	FCC + BCC	0.376	FCC + BCC	Casting
74	CoCr0.5FeNiCuAl	FCC + BCC	8.00	FCC	5.440	FCC + BCC	0.069	FCC	0.008	FCC + BCC	0.375	FCC + BCC	Casting
75	CoCrFe0.5NiCuAl	FCC + BCC	7.82	FCC + BCC	5.404	FCC + BCC	0.068	FCC	0.008	FCC + BCC	0.367	FCC + BCC	Casting
76	CoCrFeNi0.5CuAl	FCC + BCC	7.64	FCC + BCC	5.427	FCC + BCC	0.069	FCC	0.008	FCC + BCC	0.372	FCC + BCC	Casting
77	TiCr0.5FeNiCuAl	FCC + BCC	7.09	BCC	7.099	BCC	0.113	FCC + BCC	0.017	BCC	0.806	BCC	Casting
78	TiCrFeNiCuAl	FCC + BCC	7.00	BCC	7.009	BCC	0.111	FCC + BCC	0.016	BCC	0.780	BCC	Casting
79	TiCr1.5FeNiCuAl	FCC + BCC	6.92	BCC	6.905	BCC	0.109	FCC + BCC	0.015	BCC	0.749	BCC	Casting
80	TiCr2FeNiCuAl	FCC + BCC	6.86	BCC	6.794	BCC	0.106	FCC + BCC	0.014	BCC	0.717	BCC	Casting
81	TiCr3FeNiCuAl	FCC + BCC	6.75	BCC	6.566	BCC	0.099	FCC + BCC	0.013	BCC	0.652	BCC	Casting
82	TiCoCrFeNiCuAl	FCC + BCC	7.29	BCC	6.778	BCC	0.105	FCC + BCC	0.015	BCC	0.712	BCC	Casting
83	CoCrFeNiCuAlV	FCC + BCC	7.43	BCC	4.954	FCC + BCC	0.057	FCC	0.007	FCC + BCC	0.282	FCC + BCC	Casting
84	Ti0.5Co1.5CrFeNiAl	FCC + BCC	7.08	BCC	6.536	BCC	0.099	FCC + BCC	0.013	BCC	0.644	BCC	Casting
85	Ti0.5Co2CrFeNiAl	FCC + BCC	7.23	BCC	6.364	BCC	0.094	FCC + BCC	0.012	BCC	0.597	BCC	Casting
86	Ti0.5Co3CrFeNiAl	FCC + BCC	7.47	BCC	6.050	BCC	0.085	FCC	0.011	BCC	0.516	BCC	Casting
87	FeNiCrCuAl	FCC + BCC	7.60	FCC + BCC	5.628	BCC	0.073	FCC	0.009	FCC + BCC	0.413	BCC	Casting
88	FeNiCrCuMn	FCC + BCC	8.40	FCC	3.198	FCC	0.023	FCC	0.003	FCC	0.075	FCC	Casting
89	AlCoCrCuFeNi	FCC + BCC	7.83	FCC + BCC	5.281	FCC + BCC	0.065	FCC	0.008	FCC + BCC	0.344	FCC + BCC	Casting

Table II. Continued

Sl No	Systems	Exp Phase	VEC	Predicted	Atomic Mis	Predicted	Entpmis	Predicted	Eng*Smis	Predicted	Atm*Smis	Predicted	Synthesis Route
90	AlCoCrFeNi	FCC + BCC	7.20	BCC	5.778	BCC	0.078	FCC	0.009	FCC + BCC	0.449	BCC	Casting
91	AlCrFeCoNiCuMn	FCC + BCC	7.71	FCC + BCC	5.183	FCC + BCC	0.062	FCC	0.009	FCC + BCC	0.320	FCC + BCC	Casting
92	AlCrFeCoNiCuTi	FCC + BCC	7.29	BCC	6.778	BCC	0.105	FCC + BCC	0.015	BCC	0.712	BCC	Casting
93	CrCuMnNi	FCC + BCC	8.50	FCC	3.271	FCC	0.024	FCC	0.004	FCC	0.079	FCC	MA
94	AlCrCuFeNiZn	FCC + BCC	8.33	FCC	5.898	BCC	0.079	FCC	0.010	FCC + BCC	0.465	BCC	MA
95	AlCoCrCuNiZn	FCC + BCC	8.50	FCC	5.788	BCC	0.076	FCC	0.010	BCC	0.440	BCC	MA
96	Al2.5CoCrFeNi	BCC	6.23	BCC	6.842	BCC	0.105	FCC + BCC	0.013	BCC	0.719	BCC	Casting
97	Al3CoCrFeNi	BCC	6.00	BCC	6.916	BCC	0.107	FCC + BCC	0.014	BCC	0.738	BCC	Casting
98	Al0.45FeTiCrZnCu	BCC	7.77	FCC + BCC	6.693	BCC	0.100	FCC + BCC	0.013	BCC	0.669	BCC	MA
99	Al2.5FeTiCrZnCu	BCC	6.47	BCC	6.451	BCC	0.091	FCC + BCC	0.011	BCC	0.586	BCC	MA
100	Al5FeTiCrZnCu	BCC	5.60	BCC	5.953	BCC	0.076	FCC	0.008	FCC + BCC	0.454	BCC	MA
101	AlFe0.45TiCrZnCu	BCC	7.27	BCC	6.486	BCC	0.093	FCC + BCC	0.012	BCC	0.601	BCC	MA
102	AlFeTi0.45CrZnCu	BCC	7.67	FCC + BCC	6.409	BCC	0.092	FCC + BCC	0.011	BCC	0.588	BCC	MA
103	AlFeTiCr0.45ZnCu	BCC	7.47	BCC	6.562	BCC	0.095	FCC + BCC	0.012	BCC	0.622	BCC	MA
104	AlFeTiCrZn0.45Cu	BCC	6.86	BCC	6.913	BCC	0.106	FCC + BCC	0.014	BCC	0.736	BCC	MA
105	AlFeTiCrZnCu0.45	BCC	6.96	BCC	6.787	BCC	0.101	FCC + BCC	0.011	BCC	0.687	BCC	MA
106	Cu0.45NiCoZnAlTi	BCC	7.88	FCC + BCC	6.671	BCC	0.098	FCC + BCC	0.015	BCC	0.653	BCC	MA
107	Ni0.45FeCrCoMnW	BCC	7.43	BCC	4.204	FCC	0.040	FCC	0.011	BCC	0.168	FCC	MA
108	Fe0.45NiMnAlCrCo	BCC	7.08	BCC	5.649	BCC	0.073	FCC	0.010	BCC	0.411	BCC	MA
109	Fe2.5NiMnAlCrCo	BCC	7.33	BCC	5.293	FCC + BCC	0.065	FCC	0.008	FCC + BCC	0.343	FCC + BCC	MA
110	Fe5NiMnAlCrCo	BCC	7.50	FCC + BCC	4.849	FCC + BCC	0.055	FCC	0.006	FCC + BCC	0.266	FCC + BCC	MA
111	AlCrCuFeMo0.25	BCC	6.94	BCC	5.874	BCC	0.079	FCC	0.012	BCC	0.463	BCC	MA
112	AlCoCrCuFeMo0.25	BCC	7.33	BCC	5.561	BCC	0.071	FCC	0.010	BCC	0.397	BCC	MA
113	AlCoCrCuFeMo0.5	BCC	7.27	BCC	5.533	BCC	0.070	FCC	0.011	BCC	0.389	BCC	MA
114	Al2CoCrCuFeNi	BCC	7.14	BCC	6.257	BCC	0.089	FCC	0.011	BCC	0.559	BCC	Casting
115	Al2CoCrFeNi	BCC	6.50	BCC	6.678	BCC	0.101	FCC + BCC	0.013	BCC	0.675	BCC	Casting
116	Ti2CrFeCoNiAl	BCC	6.29	BCC	7.645	BCC	0.130	FCC + BCC	0.019	BCC	0.995	BCC	Casting
117	Ti3CrFeCoNiAl	BCC	6.00	BCC	7.723	BCC	0.131	FCC + BCC	0.020	BCC	1.012	BCC	Casting
118	CrFeCoNiAlCu0.25	BCC	7.38	BCC	5.641	BCC	0.074	FCC	0.009	FCC + BCC	0.418	BCC	Casting
119	Ti0.5CrFeCoNiAl0.75Cu0.25	BCC	7.27	BCC	6.381	BCC	0.094	FCC + BCC	0.013	BCC	0.602	BCC	Casting
120	Al0.5CoCrCuFeNiTi1.2	BCC	7.51	FCC + BCC	6.756	BCC	0.105	FCC + BCC	0.015	BCC	0.710	BCC	Casting
121	Al0.5CoCrCuFeNiTi1.4	BCC	7.41	BCC	6.938	BCC	0.110	FCC + BCC	0.016	BCC	0.765	BCC	Casting
122	Al0.5CoCrCuFeNiTi1.6	BCC	7.31	BCC	7.086	BCC	0.115	FCC + BCC	0.017	BCC	0.812	BCC	Casting
123	Al0.5CoCrCuFeNiTi1.8	BCC	7.22	BCC	7.209	BCC	0.118	FCC + BCC	0.018	BCC	0.851	BCC	Casting
124	Al0.5CoCrCuFeNiTi2	BCC	7.13	BCC	7.309	BCC	0.121	FCC + BCC	0.019	BCC	0.884	BCC	Casting
125	Al0.5CrFe1.5MnNi1.5	BCC	7.55	FCC + BCC	4.872	FCC + BCC	0.055	FCC	0.008	FCC + BCC	0.267	FCC + BCC	Casting
126	Ti0.5CrFeNiAlCo	BCC	6.91	BCC	6.718	BCC	0.104	FCC + BCC	0.014	BCC	0.696	BCC	Casting
127	Al2.5FeNiCrCuCo	BCC	6.87	BCC	6.478	BCC	0.095	FCC + BCC	0.012	BCC	0.616	BCC	MA
128	Al5FeNiCrCuCo	BCC	5.90	BCC	6.701	BCC	0.099	FCC + BCC	0.013	BCC	0.663	BCC	MA
129	AlCoCrFe0.6Mo0.5Ni	BCC	7.02	BCC	5.852	BCC	0.079	FCC	0.013	BCC	0.460	BCC	Casting
130	AlCoCrFeMo0.5Ni	BCC	7.09	BCC	5.755	BCC	0.076	FCC	0.012	BCC	0.439	BCC	Casting
131	AlCoCrFe1.5Mo0.5Ni	BCC	7.17	BCC	5.631	BCC	0.073	FCC	0.011	BCC	0.413	BCC	Casting
132	AlCoCrFe2Mo0.5Ni	BCC	7.23	BCC	5.508	BCC	0.070	FCC	0.010	BCC	0.388	BCC	Casting
133	AlFe	BCC	5.50	BCC	7.146	BCC	0.112	FCC + BCC	0.012	BCC	0.803	BCC	MA
134	AlFeTi	BCC	5.00	BCC	7.101	BCC	0.108	FCC + BCC	0.013	BCC	0.767	BCC	MA

Table II. Continued

Sl No	Systems	Exp Phase	VEC	Predicted	Atomic Mis	Predicted	Entpmis	Predicted	Eng*Smis	Predicted	Atm*Smis	Predicted	Synthesis Route
135	AlFeTiCr	BCC	5.25	BCC	7.548	BCC	0.125	FCC + BCC	0.013	BCC	0.946	BCC	MA
136	AlFeTiCrZn	BCC	6.60	BCC	6.856	BCC	0.103	FCC + BCC	0.010	BCC	0.703	BCC	MA
137	AlFeTiCrZnCu	BCC	5.83	BCC	6.984	BCC	0.107	FCC + BCC	0.014	BCC	0.750	BCC	MA
138	FeTiCrZnCu	BCC	8.20	FCC	6.641	BCC	0.099	FCC + BCC	0.013	BCC	0.659	BCC	MA
139	CuNiCoZnAlTi	BCC	8.17	FCC	6.577	BCC	0.096	FCC + BCC	0.015	BCC	0.631	BCC	MA
140	NiCoZnAlTi	BCC	7.60	FCC + BCC	6.725	BCC	0.099	FCC + BCC	0.015	BCC	0.664	BCC	MA
141	NiFeCrCoMnW	BCC	7.67	FCC + BCC	4.127	FCC	0.039	FCC	0.010	BCC	0.159	FCC	MA
142	FeCrCoMnW	BCC	7.20	BCC	4.257	FCC	0.041	FCC	0.011	BCC	0.174	FCC	MA
143	FeNiMnAl	BCC	7.00	BCC	6.017	BCC	0.081	FCC	0.012	BCC	0.489	BCC	MA
144	FeNiMnAlCr	BCC	6.80	BCC	5.828	BCC	0.077	FCC	0.010	BCC	0.449	BCC	MA
145	FeNiMnAlCrCo	BCC	7.17	BCC	5.566	BCC	0.071	FCC	0.010	BCC	0.395	BCC	MA
146	NiMnAlCrCo	BCC	7.00	BCC	5.699	BCC	0.074	FCC	0.011	BCC	0.421	BCC	MA
147	AlCoCrCuFe	BCC	7.40	BCC	5.580	BCC	0.072	FCC	0.009	FCC + BCC	0.403	BCC	MA
148	AlCuCrFe	BCC	7.00	BCC	5.957	BCC	0.081	FCC	0.010	FCC + BCC	0.485	BCC	MA
149	AlCrCoFe	BCC	6.50	BCC	6.201	BCC	0.089	FCC	0.010	BCC	0.549	BCC	MA
150	TiCrFeCoNiAl	BCC	6.67	BCC	7.221	BCC	0.118	FCC + BCC	0.017	BCC	0.854	BCC	Casting

favored by lower values ($\delta < 5$ favors the FCC and $\delta > 5.4$ favors the BCC). The same trend can be seen for S_σ as $S_\sigma < 0.06$ favors the FCC and $S_\sigma > 0.07$ favors the BCC. These two values are misfit parameters which indicate the strain in the system and the loss in overall configurational entropy due to the difference in the size of the constituent elements, respectively. Higher value of δ means the system possesses more strain energy and to relieve itself from this it tends to attain more open structure, *i.e.*, the BCC structure.

The plot for electronegativity difference does not show very clear demarcation of phases. All the systems have values nearly in the range of 0.09 to 0.17 as only metals are involved.

Figures 2(a) and (b) presents the 1D maps of the computed values of ΔS_{mix} and ΔS_{f}, respectively. The computed plots of ΔS_{mix} and ΔS_{f} do not shed much light upon the phase regime demarcation, as all the three phases share almost equal values for both the parameters. This is because the ΔS_{mix} is only dependent upon the number of different elements present in the system and does not take into account the nature of the elements. Similarly, according to Richard's rule,[21] the entropy change per mole, ΔS_{f}, during solid-to-liquid transformation is approximately one gas constant R (magnitude wise) for all the systems irrespective of the crystal structure.

Two new parameters which have been introduced here are the Modified Darken–Gurry parameter ($\mathbf{A} = \boldsymbol{S_\sigma} * \chi$) and a Modified Mismatch Entropy parameter ($\mathbf{B} = \boldsymbol{\delta} * \boldsymbol{S_\sigma}$). The 1D maps of these parameters for various HEA systems have been shown in Figure 3. It can be clearly seen that for alloys with values of $A > 0.0095$, BCC is the stable crystal structure and those with $A < 0.0060$, FCC is the stable phase. The Modified Darken–Gurry parameter has actually been derived from the concept of Darken–Gurry (DG) maps[31,44] which takes into account the simultaneous effect of the difference in atomic size and electronegativity of various elements on solid solution formation. These maps basically consist of atomic size on abscissa and electronegativity on the ordinate axes where any element can be represented by a point, and if two points lie close to each other, then they tend to form solid solutions across a wide composition range. The justification for this lays in the small difference in the atomic size and electronegativities of the different components tending the system towards a solid solution. The points which are positioned far on such a plot would implicate that the corresponding components would either tend to form intermetallic or an amorphous phase in the solid state. However, in the present work, the aim is to explore within the solid solution regime of various elements on respective DG maps, whether there is any presence of crystal structure-based demarcation. For this, atomic size has been replaced by mismatch entropy so as to render more thermodynamic analogy to the parameter and its product with electronegativity difference has been considered so that an area on the DG map could be reflected. Now, as the value of A is lower for a particular multicomponent system, the difference in electronegativities of the constituent components as well

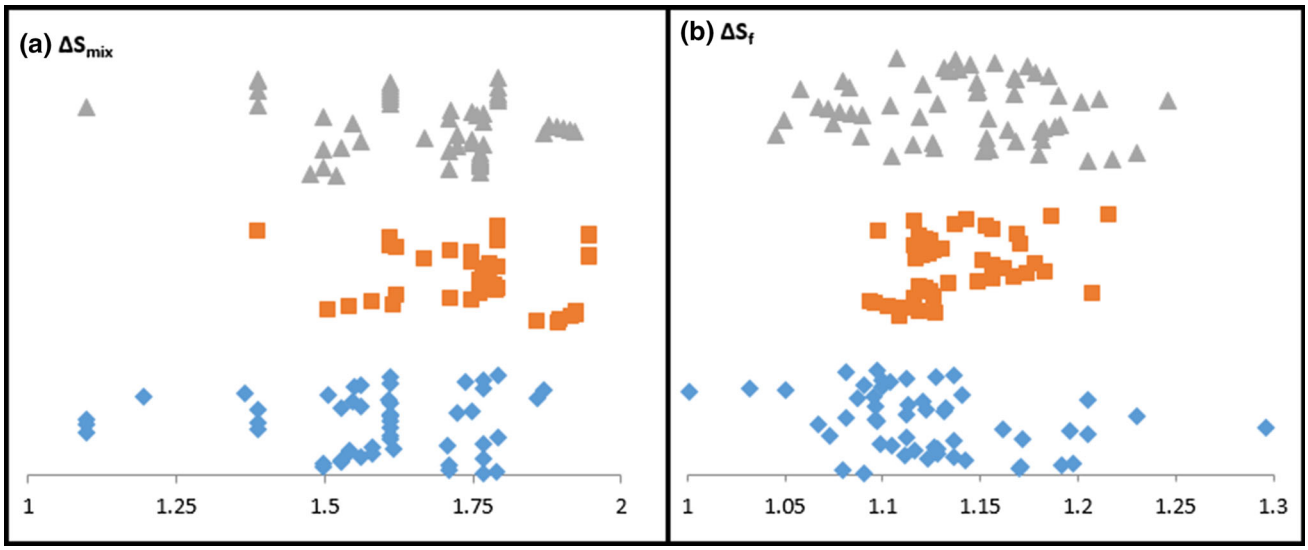

Fig. 2—1D maps of the computed values of (*a*) ΔS_{mix} and (*b*) ΔS_f.

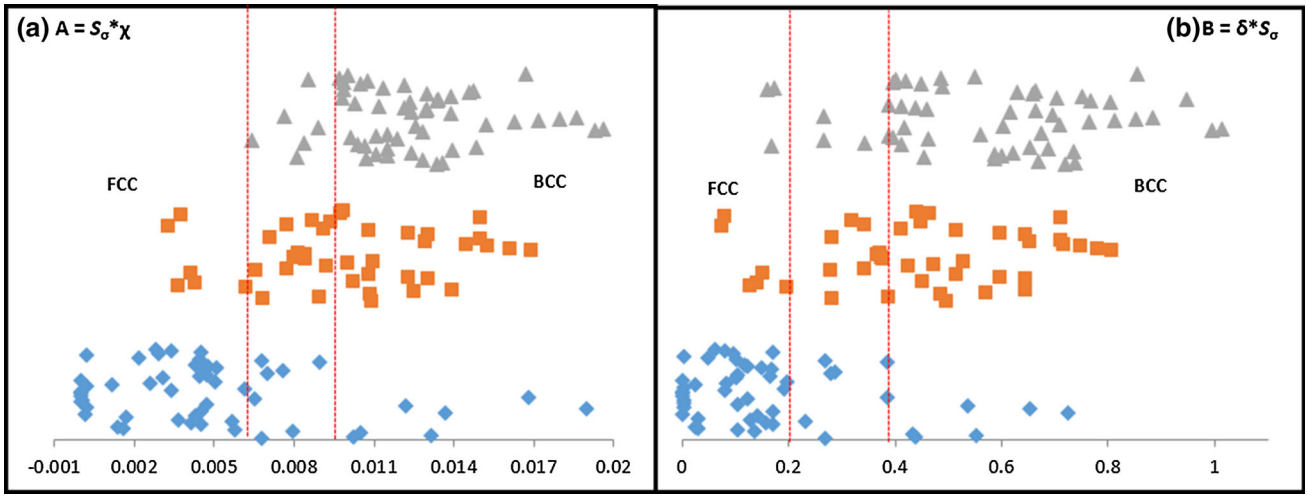

Fig. 3—1D maps of the computed values of (*a*) A = S_σ *χ and (*b*) B = δ^* S_σ.

as the overall mismatch entropy is lower. Thus, the system is on the lower side of residual strain (due to atomic size mismatch) and with a nearly equivalent affinity of each component for the rest, tends to form a solid solution with the closest packed structure. However, when the value of A is higher yet in the regime of solid solution for the respective components on the DG map, the system tends to opt for a rather open structure so as to accommodate the strain coming from atomic size mismatch and to reduce the difference in affinity of each component for the rest. This trend of stable structure prediction can also be thought of in terms of an energy minimization notion. The ground-state structure has to be such that it minimizes the strain energy as well as electronic kinetic energy. In case of the high value of A, where the mismatch entropy and the difference in electronegativity are high, the BCC structure would be preferred as the default presence of components with higher affinity for electrons would lower the kinetic energy and an open structure would relax the strain energy due to size mismatch. On the other hand in case of a lower value of A, there would be a requirement of a close packed structure (FCC) for an overall lowering of the electronic kinetic energy.

Similarly, for alloys with values of Modified Mismatch Entropy parameter, B ($=\delta^* S_\sigma$)>0.38, the BCC phase is the stable one, whereas for $B<0.2$, FCC is the stable one. This parameter is again a product of a thermodynamic and a topological parameter which follows the same philosophy in phase demarcation as followed by δ and S_σ individually.[45] Table III shows the prediction accuracy of the various parameters which were found to be suitable for estimating the ground-state structure.

It is re-emphasized here again that in the present assessment the thresholding limits of various parameters

Table III. Overall Prediction Accuracy of Some of the Parameters Under Consideration *Viz*. VEC, Atomic Mismatch, Mismatch Entropy, Modified Darken–Gurry Paramater, and Modified Mismatch Entropy Parameter, When Calculated Across the Total Number of Systems

	Prediction Accuracy (in pct)			
Parameter	Only FCC (Pct)	FCC + BCC (Pct)	Only BCC (Pct)	Overall (Pct)
VEC	81.1	38.1	81.8	67.0
Atomic mismatch	75.4	28.5	89.0	64.3
Mismatch entropy	73.6	26.2	83.6	61.1
Modified Darken–Gurry parameter	64.1	38.1	87.2	63.1
Modified mismatch entropy parameter	75.4	23.8	89	62.7

used to demarcate different crystal structure regimes have been set keeping in view the maximum containment of either single-phase FCC or single-phase BCC exhibiting systems within the specified range. However, a close analysis of the spread of mixed FCC + BCC-containing systems (in Figure 3) reveals that in most cases both the Modified Darken–Gurry as well the Modified Mismatch Entropy parameters predict either a mixed FCC + BCC or single-phase BCC crystal structure for those systems at the ground state. This can be understood by looking at the composition of those mixed FCC + BCC containing systems, where there is presence of certain elements with highly differing atomic radius or electronegativity from the rest like Al, Ti, W, Mo, or Zn (refer Table I for values). Under these circumstances the prediction of these parameters of a mixed or rather an overall open structure is as per the explanation given above. Another observation that can be drawn from Table II and which further substantiates the aforementioned argument is that in cases where these parameters predict a mixed FCC + BCC structure, however, experimental observation differs, there lies the presence of these radius/electronegativity wise different elements. The exact concurrence between the predicted structure and the observed structure would have been possible only if there could have been a possibility of performing a robust total energy minimization scheme. However, it can still be seen that the two newly introduced metrics *viz*. Modified Darken–Gurry Parameter (A) and the Modified Mismatch Entropy Parameter (B) are reasonably capable of predicting the stable crystal structure, given it is either FCC or BCC.

- VEC accurately predicts phase selection in HEA systems to a large extent. HEAs with higher values of VEC tend to form FCC phase and those with lower values favor the BCC phase.
- The new parameters namely the Modified Darken–Gurry parameter, show that FCC is the stable for values less than 0.0060 and the BCC above 0.0095. The Modified Mismatch Parameter depicts the stable FCC below 0.2 and the stable BCC phase above 0.38.

REFERENCES

1. B. Cantor, K.B. Kim, and P.J. Warren: *Mater. Sci. Forum*, 2002, vol. 27, pp. 386–88.
2. C.Y. Hsu, J.W. Yeh, S.K. Chen, and T.T. Shun: *Metall. Mater. Trans. A*, 2004, vol. 35A, pp. 1465–69.
3. J.W. Yeh, S.K. Chen, S.J. Lin, J.Y. Gan, T.S. Chin, T.T. Shun, C.H. Tsau, and S.Y. Chang: *Adv. Eng. Mater.*, 2004, vol. 6, pp. 299–303.
4. B. Cantor: *Entropy*, 2014, vol. 16, pp. 4749–68.
5. Y. Zhang, T.T. Zuo, Z. Tang, M.C. Gao, K.A. Dahmen, P.K. Liaw, and Z.P. Lu: *Prog. Mater. Sci.*, 2014, vol. 61, pp. 1–93.
6. Y. Zhang, Y.J. Zhou, and J.P. Lin: *Adv. Eng. Mater.*, 2008, vol. 10, pp. 534–38.
7. R. Raghavan, K.C. Hari Kumar, and B.S. Murty: *J. Alloys Compd.*, 2012, vol. 544, pp. 152–58.
8. D.J.M. King, S.C. Middleburgh, A.G. McGregor, and M.B. Cortie: *Acta Mater.*, 2016, vol. 104, pp. 172–79.
9. S. Guo, C. Ng, J. Lu, and C.T. Liu: *J. Appl. Phys.*, 2011, vol. 109, pp. 103505 (1-5).
10. S. Guo: *Mater. Sci. Technol.*, 2015, DOI:10.1179/1743284715y.0000000018.
11. S. Guo and C.T. Liu: *Prog. Nat. Sci.: Mater. Int.* 2011, vol. 21, pp. 433–46.
12. A. Takeuchi and A. Inoue: *Intermetallics*, 2010, vol. 18, pp. 1779–89.
13. A. Takeuchi and A. Inoue: *Mater. Trans.*, 2000, vol. 41, pp. 1372–78.
14. X. Yang and Y. Zhang: *Mater. Chem. Phys.*, 2012, vol. 132, pp. 233–38.
15. Y.F. Ye, Q. Wang, J. Lu, C.T. Lu, and Y. Yang: *Scr. Mater.*, 2015, vol. 104, pp. 53–55.
16. Y. Zhang, S. Guo, C.T. Liu, and X. Yang: in *High-Entropy Alloys*, M.C. Gao, J.W. Yeh, P.K. Liaw, and Y. Zhang, eds., Springer, Switzerland, 2016, pp. 21–50.
17. Y.F. Ye, Q. Wang, J. Lu, C.T. Lu, and Y. Yang: *Intermetallics*, 2015, vol. 59, pp. 75–80.
18. M. Widom: in *High-Entropy Alloys*, M.C. Gao, J.W. Yeh, P.K. Liaw, and Y. Zhang, eds., Springer, Switzerland, 2016, pp. 267–98.
19. F. Tian, Y. Wang, D.L. Irving, and L. Vitos: in *High-Entropy Alloys*, M.C. Gao, J.W. Yeh, P.K. Liaw, and Y. Zhang, eds., Springer, Switzerland, 2016, pp. 299–332.
20. M.C. Gao, C. Niu, C. Jiang, and D.L. Irving: in *High-Entropy Alloys*, M.C. Gao, J.W. Yeh, P.K. Liaw, and Y. Zhang, eds., Springer, Switzerland, 2016, pp. 333–68.
21. M.C. Gao: in *High-Entropy Alloys*, M.C. Gao, J.W. Yeh, P.K. Liaw, and Y. Zhang, eds., Springer, Switzerland, 2016, pp. 369–98.
22. C. Zhang and M.C. Gao: in *High-Entropy Alloys*, M.C. Gao, J.W. Yeh, P.K. Liaw, and Y. Zhang, eds., Springer, Switzerland, 2016, pp. 399–444.
23. W. Kohn and L.J. Sham: *Phys. Rev.*, 1965, vol. 140 (1965), pp. A1133–38.
24. N. Saunders and A.P. Miodownik: *CALPHAD A Comprehensive Guide*. Pergamon Materials Series, vol. 1, Elsevier Science Ltd., UK, 1998, pp. 91–124.
25. A. Takeuchi and A. Inoue: *Mater. Sci. Eng. A*, 2001, vol. 446, pp. 304–06.
26. Extended information on TCHEA2—TCS High Entropy Alloy Database Version 2.0, https://www.thermocalc.com/products-services/databases/thermodynamic/.
27. M.C. Gao, B. Zhang, S.M. Guo, J.W. Qiao, and J.A. Hawk: *Metall. Mater. Trans. A*, 2016, DOI:10.1007/s11661-015-3091-1.
28. F. Otto, Y. Yang, H. Bei, and E.P. George: *Acta Mater.*, 2013, vol. 61, pp. 2628–38.

29. B.S. Murty, J.W. Yeh, and S. Ranganathan: *High Entropy Alloys*, Butterworth-Heinemann, Elsevier, 2014, pp. 37–56.
30. W. Hume Rothery: *Atomic Theory for Students of Metallurgy*, Institute of Metals: Monograph and Report No. 3, 1948, pp. 179–208.
31. R.W. Cahn and P. Hassen: *Physical Metallurgy*, 4th edn., Elsevier Science B.V., North Holland, 1996, pp. 47–203.
32. T.Y. Egami and Y. Waseda: *J. Non-Cryst. Solids*, 1984, vol. 64, pp. 113–34.
33. D.B. Miracle: *Acta Mater.*, 2006, vol. 54, pp. 4317–36.
34. D.B. Miracle, J.D. Miller, O.N. Senkov, C. Woodward, M.D. Uchic, and J. Tiley: *Entropy*, 2014, vol. 16, pp. 494–525.
35. O.N. Senkov and D.B. Miracle: *Mater. Res. Bull.*, 2001, vol. 36, pp. 2183–98.
36. R. Sriharitha, B.S. Murty, and R.S. Kottada: *Intermetallics*, 2013, vol. 32, pp. 119–26.
37. F.J. Wang, Y. Zhang, and G.L. Chen: *J. Alloys Compd.*, 2009, vol. 478, pp. 321–24.
38. X.F. Wang, Y. Zhang, Y. Qiao, and G.L. Chen: *Intermetallics*, 2007, vol. 15, pp. 357–62.
39. C. Li, J.C. Li, M. Zhao, and Q. Jiang: *J. Alloys Compd.*, 2009, vol. 475, pp. 752–7.
40. S. Varalakshmi, M. Kamaraj, and B.S. Murty: *Metall. Mater. Trans. A*, 2010, vol. 41A, pp. 2703–09.
41. T.T. Shun, C.H. Hung, and C.F. Lee: *J. Alloys Compd.*, 2010, vol. 495, pp. 55–8.
42. U. Mizutani: *Hume Rothery Rules for Structurally Complex Alloy Phases*, CRC Press, Taylor & Francis Group, Boca Raton, 2011, pp. 21–48.
43. G.A. Mansoori, N.F. Carnahan, K.E. Starling, and T.W. Leland, Jr: *J. Chem. Phys.*, 1971, vol. 54, pp. 1523–25.
44. L.S. Darken and K.W. Gurry: *Physical Chemistry of Metals*, CBS Publishers, McGraw-Hill, NY, 2002, pp. 74–109.
45. A. Takeuchi, K. Amiya, T. Wada, K. Yubuta, W. Zhang, and A. Makino: *Entropy*, 2013, vol. 15, pp. 3810–21.